Please verify that (1) all pages are present, (2) all figures are acceptable, (3) all fonts and special characters are correct, and (4) all text and figures fit within the margin lines shown on this review document. Return to your MySPIE ToDo list and approve or disapprove this submission.

Plasmon-resonant nanorods as multimodal agents for two-photon luminescent imaging and photothermal therapy

Terry B. Huff[a], Matthew N. Hansen[a], Ling Tong[a], Yan Zhao[a], Haifeng Wang,[b] Daniel A. Zweifel,[a] Ji-Xin Cheng[a,b], and Alexander Wei[a,*]

[a]Department of Chemistry and [b]Department of Biomedical Engineering, Purdue University, West Lafayette, IN 47907

ABSTRACT

Plasmon-resonant gold nanorods have outstanding potential as multifunctional agents for image-guided therapies. Nanorods have large absorption cross sections at near-infrared (NIR) frequencies, and produce two-photon luminescence (TPL) when excited by fs-pulsed laser irradiation. The TPL signals can be detected with single-particle sensitivity, enabling nanorods to be imaged *in vivo* while passing through blood vessels at subpicomolar concentrations. Furthermore, cells labeled with nanorods become highly susceptible to photothermal damage when irradiated at plasmon resonance, often resulting in a dramatic blebbing of the cell membrane. However, the straightforward application of gold nanorods for cell-specific labeling is obstructed by the presence of CTAB, a cationic surfactant carried over from nanorod synthesis which also promotes their nonspecific uptake into cells. Careful exchange and replacement of CTAB can be achieved by introducing oligoethyleneglycol (OEG) units capable of chemisorption onto nanorod surfaces by *in situ* dithiocarbamate formation, a novel method of surface functionalization. Nanorods with a dense coating of methyl-terminated OEG chains are shielded from nonspecific cell uptake, whereas nanorods functionalized with folate-terminated OEG chains accumulate on the surface of tumor cells overexpressing their cognate receptor, with subsequent delivery of photoinduced cell damage at low laser fluence.

Keywords: Contrast agents, nonlinear optics, photothermolysis, plasmon resonance, two-photon luminescence

* E-mail: alexwei@purdue.edu; Tel: +1 765 494 5257; http://www.chem.purdue.edu/awei

1. INTRODUCTION

Anisotropic gold nanoparticles are ideally suited as contrast agents for optical imaging of biological tissues. Colloidal gold is essentially inert and has a long history of clinical use, but can also be engineered into nanostructured forms with surface plasmon modes ranging from visible to near-infrared (NIR) wavelengths. The NIR region between 750 and 1300 nm is particularly favorable for optical imaging, as shorter wavelengths are extinguished by hemoglobin or other endogenous pigments, and longer wavelengths are strongly attenuated by water.[1] Several types of NIR-resonant gold nanoparticles are currently being investigated as contrast agents for various biomedical imaging modalities, including nanoshells,[2,3] nanocages,[4] and nanorods.[5] The latter are especially attractive for such applications, as they can support a higher absorption cross section at NIR frequencies per unit volume than most other structures, and have narrower linewidths at comparable resonance frequencies due to reduced radiative damping effects.[6] Nanorods are efficiently prepared in micellar surfactant solutions using seeded growth conditions,[7,8] but this approach is often accompanied by a drift in the nanorods' plasmon resonance frequency over time, due to a gradual reshaping by a slow growth process. Fortunately, this is easily remedied by treating freshly prepared nanorods with sodium sulfide to stabilize them against such "optical drift," thereby facilitating their practical application as NIR contrast agents.[9]

Gold nanoparticles are most commonly visualized by resonant light scattering, which is enhanced by orders of magnitude when excited at specific plasmon modes. However, the particles' scattering cross sections scale geometrically as a function of particle volume, whose upper size limit is determined by issues of biocompatibility for particles whose dimensions exceed 100 nm. Other optically induced imaging modalities are currently being explored; for example, plasmon-resonant nanoparticles have been shown to be effective at transducing light absorption into heat, and are being developed as photothermal contrast agents for magnetic resonance imaging[10] and optoacoustic tomography.[3]

SPIE USE: ____ DB Check, ____ Prod Check, Notes:

Please verify that (1) all pages are present, (2) all figures are acceptable, (3) all fonts and special characters are correct, and (4) all text and figures fit within the margin lines shown on this review document. Return to your MySPIE ToDo list and approve or disapprove this submission.

Here we describe some recent progress in biological imaging with gold nanorods based on their two-photon luminescence (TPL).[11,12] This is an unusual property for metal nanoparticles, which are better known for their efficacy in fluorescence quenching; nevertheless, gold nanorods are capable of producing strong TPL signals under femtosecond-pulsed laser excitation conditions, and can be imaged with single-particle sensitivity. The nanorods' intrinsic TPL properties are useful for real-time imaging *in vitro* and *in vivo*, as demonstrated by characterization of their uptake into cells[13] and by monitoring their blood residency in animal models.[11] Most recently, we have found gold nanorods to be highly potent agents for mediating the photothermal destruction of tumor cells, and have used TPL to obtain insights into their ability to inflict photoinduced injury.[14] As a corollary to these studies, we have determined that control over the nanorods' surface chemistry is critical to their successful development as multifunctional agents for targeted imaging and therapy, and have developed a robust, one-step method of surface functionalization based on the *in situ* formation of dithiocarbamate (DTC) ligands, derived from the corresponding amines.[13-15]

2. EXPERIMENTAL SECTION

2.1 Synthesis and functionalization of gold nanorods

Gold nanorods were prepared in high yields in the presence of cetyltrimethylammonium bromide (CTAB) and silver nitrate using the seeded growth conditions described by Sau and Murphy,[7b] and treated with sodium sulfide 15-30 minutes after injection of the seed solution to arrest further growth.[9] The sulfide-treated nanorods possess a dumbbell-like geometry with slightly flared ends, and exhibited longitudinal plasmon resonances ranging from 765 and 820 nm which were optically stable over time. These NIR-resonant nanorods were typically produced with lengths of 45-50 nm and aspect ratios between 3 and 4. The nanorods were centrifuged and redispersed in deionized water two times (24000 *g*, 5 min per cycle) to remove most of the CTAB and residual metal sulfide, and diluted to an optical density in the range of 1.0 to 1.2 (see Figure 1).

To prepare oligoethyleneglycol-coated nanorods, CTAB-coated nanorods were first conditioned with a mixed-bed ion-exchange resin (Amberlite MB-3, Sigma) at room temperature for several hours to remove unassociated surfactant and other ions.[16] Nanorods were then decanted and redispersed into a 2% solution of methyl-terminated polyethylene-glycolamine (mPEG-amine, Nektar) or *O,O*'-bis(2-aminoethyl)octadecaethylene glycol (OEG-diamine, Fluka) adjusted to pH 9.5, followed by a saturated aqueous solution of freshly distilled CS_2 for *in situ* DTC formation. The mixtures were stirred for 12 hours, then subjected to membrane dialysis for 2 hours (MW cutoff = 6000-8000) to produce stable dispersions of mPEG- or amino-OEG-coated nanorods. Treatment of the latter with a 10-μM DMSO solution of *N*-hydroxysuccinimidyl folate (NHS-folate) followed by additional dialysis yielded a stable dispersion of folate-conjugated nanorods.[14] It is worth mentioning that the displacement of CTAB by the OEG-DTC ligands often results in a slight redshift in the nanorod absorption peak, due to the highly sensitive nature of its longitudinal plasmon resonance to changes in the surface dielectric.[9,17]

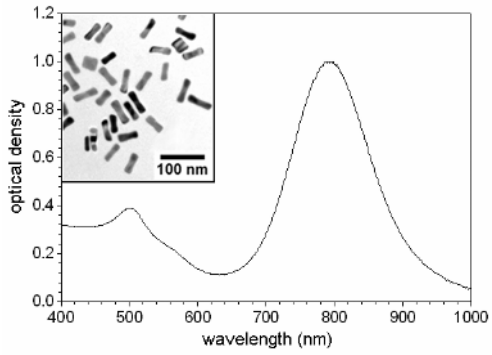

Figure 1. Extinction spectrum of CTAB-stabilized gold nanorods with a longitudinal plasmon mode centered at 790 nm and a transverse mode centered at 505 nm. *Inset*: TEM image of nanorods (JEOL 2000FX, 200kV).

SPIE USE: ____ DB Check, ____ Prod Check, Notes:

Please verify that (1) all pages are present, (2) all figures are acceptable, (3) all fonts and special characters are correct, and (4) all text and figures fit within the margin lines shown on this review document. Return to your MySPIE ToDo list and approve or disapprove this submission.

2.2 TPL imaging and single-particle tracking analysis

A femtosecond (fs) Ti:Sapphire laser (Mira 900, Coherent, Santa Clara, CA) was used to generate laser pulses with a duration of 200 fs at a repetition rate of 77 MHz, tuned to the nanorods' plasmon resonance for optimal two-photon excitation, with an incident power of 1-2 mW at the sample. The laser beam was directed into a scanning confocal microscope (FV300/IX70, Olympus, Melville, NY) equipped with a 60X water-immersion objective (N.A.=1.2). Consecutive real-time images (movies) were recorded at a speed of 0.6 frames per second, using the transmission signal to visualize the KB cells. FluoView software (Olympus, Tokyo, Japan) was used to convert time-lapsed TPL images (movies) to a series of 8-bit TIFF files. The image pixel sizes were adjusted to a spatial resolution suitable for tracking individual nanorods, which could be readily identified after appropriate parameterization of particle size, eccentricity, and total and mean intensities. The centroid of a given nanorod could be determined with sub-pixel resolution by fitting its intensity profile to a Gaussian distribution; trajectories were produced by correlating changes in centroid positions between adjacent frames. Nanorod movement was characterized by its instantaneous velocity, calculated as the displacement divided by the time interval between two adjacent frames. Plus and minus velocities indicated nanorod movement towards the cell periphery and the nucleolus, respectively.

2.3 *In vitro* and *in vivo* TPL imaging studies

Studies involving nanorod cell uptake and subsequent photothermolysis were conducted using adherent KB cells (a tumor cell line derived from oral epithelium which overexpresses the high-affinity folate receptor), which were treated with 100-μL aliquots of nanorod solutions (O.D. ~1) in serum-free RPMI growth medium and maintained under standard cell growth conditions prior to examination. Cells were washed with fresh RPMI growth medium to remove free nanorods prior to TPL imaging, which was performed on an inverted microscope with a 60X water objective (N.A.=1.2). Cells in a selected area (~ 40 × 40 μm) were scanned continuously for 30 s using a scan rate of 1.66 s. Photothermolysis was performed in continuous-wave mode under constant average power, ranging from 7.5 to 60 mW at the sample. The mean power density was calculated by dividing the average laser power with the scanning area. The focal spot area was calculated as $\pi d^2/4$, where $d = 0.61\ \lambda/NA$ is the full width at half maximum of the beam waist. Each scan was digitized into 512 × 512 pixels (pixel area = 77 × 77 nm^2; exposure time = 6.3 μs per pixel per scan). The exposure time for a nanorod per scan was approximated as (focal spot area / pixel area) × 6.3 μs = 0.126 ms; the total exposure time was calculated as (0.126 ms × total scan time /scan rate) = 2.28 ms, and the laser fluence was determined as (mean power density / total exposure time).

In vivo studies were conducted using a 6-8 week-old Balb/C (nude) female mouse, anesthetized by intraperitoneal injection of avertin (500 mg/kg) prior to tail vein injection of a 200-μL aliquot of nanorods (O.D.~0.2, diluted 1:4 with PBS buffer). The mouse was placed on a Petri dish with one ear attached to the coverslip bottom, using glycerol as an interstitial medium to reduce optical interference. A 40X water-immersion objective with a working distance of 3.3 mm was used to focus the laser beam onto the ear lobe. The laser power at the sample was approximately 18 mW.

3. RESULTS AND DISCUSSION

3.1 Characterization of TPL in gold nanorods

Two-photon luminescence from gold has been previously observed, and was first characterized by Mooradian.[18] TPL can be described as a three-step process: (i) excitation of electrons from the *d*- to the *sp*-band to generate electron–hole pairs, (ii) scattering of electrons and holes on the picosecond timescale with partial energy transfer to the phonon lattice, and (iii) electron–hole recombination resulting in photon emission. The intrinsic TPL efficiency of gold is quite poor, but TPL signals from nanostructured gold can be amplified by many orders of magnitude via resonant coupling with localized surface plasmons.[19] It is therefore possible to engineer plasmon-resonant nanoparticles to produce strong TPL signals upon NIR excitation, with the greatest efficiency expected for particles having stable resonances with narrow linewidths. We have found that this is indeed the case with gold nanorods, whose plasmon resonances and emission signals are unbleached by laser irradiation at picojoule pulse energies.

Aqueous dispersions of gold nanorods were excited under fs-pulsed conditions at different NIR wavelengths to produce broad emission spectra in the visible region (see Figure 2a).[11] Several of the TPL peaks could be attributed to known interband transitions such as 6-5L (electron-hole recombination) and 6-5X, which have been correlated with emissions from bulk gold.[19] The relative peak positions in the emission spectra were largely unaffected by the choice of

SPIE USE: ____ DB Check, ____ Prod Check, Notes:

Please verify that (1) all pages are present, (2) all figures are acceptable, (3) all fonts and special characters are correct, and (4) all text and figures fit within the margin lines shown on this review document. Return to your MySPIE ToDo list and approve or disapprove this submission.

excitation frequency, but the overall TPL intensity correlated strongly with excitation wavelength and reached a maximum at plasmon resonance, indicating a plasmon-enhanced two-photon absorption cross section (see Figure 2b). Lastly, the emission intensities scaled quadratically with incident power (see Figure 2c), whereas irradiation of the nanorods at a comparable power in cw mode reduced the signal to background noise level, confirming the two-photon nature of the nanorod luminescence.

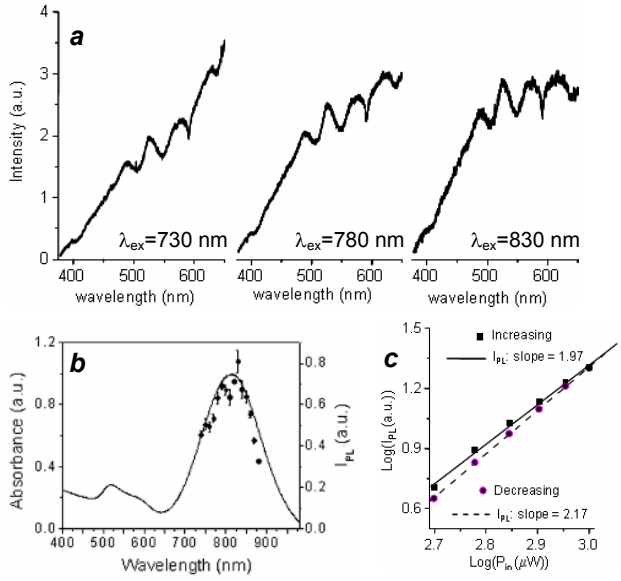

Figure 2. (a) TPL spectra from gold nanorods at three different excitation wavelengths; spectra are cut off above 660 nm by a band pass filter. (b) TPL excitation spectrum (circles with error bars, right *y*-axis) superimposed onto nanorod absorption spectrum (solid line). (c) Quadratic dependence of TPL emission intensity on excitation power. Reproduced with permission from the National Academy of Sciences.

The TPL intensities of the gold nanorods were also determined to have a strong angular dependency on the polarization of incident excitation.[11] Nanorods were dispersed and immobilized onto glass cover slips such that isolated particles could be analyzed during fs-pulsed excitation at their longitudinal plasmon resonance (see Figure 3). Strong TPL intensities were observed from single nanorods with a $\cos^4$ dependence on incident polarization, similar to that observed in the two-photon excitation of single fluorescent molecules. In contrast, the emission band was broad and essentially depolarized, confirming the incoherent nature of TPL. Comparison of the nanorods' TPL intensities with that produced by single rhodamine dye molecules[20] reveals a nearly 60-fold difference in brightness under identical excitation conditions; the two-photon cross section of the average nanorod was estimated to be more than 2000 GM.

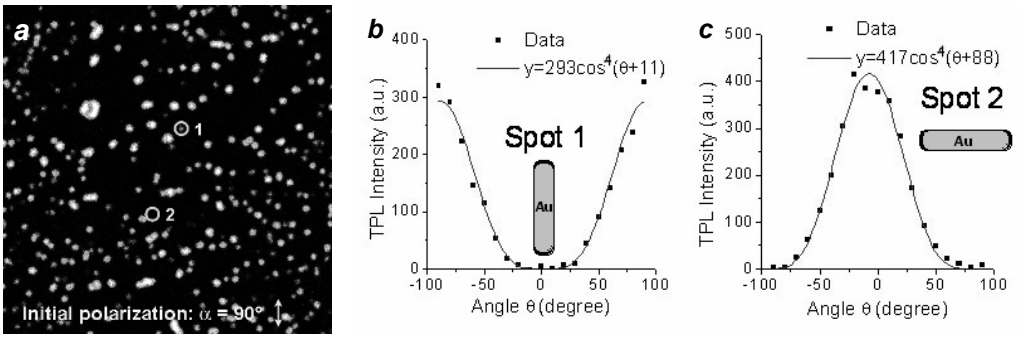

Figure 3. Polarization-dependent TPL intensities of single gold nanorods.[11] (a) Grayscale image with initially vertical excitation polarization (α=θ–180°); image size is 25 × 25 μm. Single nanorods (e.g. "1" and "2") could be identified by their similar range of intensities; brighter spots represent clusters of nanorods. (b,c) TPL intensity (solid dots) for individual nanorods located at "Spot 1" and "Spot 2" as a function of incident polarization angle. Each TPL signal fits a $\cos^4\alpha$ function. Reprinted with permission from the National Academy of Sciences.

SPIE USE: ____ DB Check, ____ Prod Check, Notes:

Please verify that (1) all pages are present, (2) all figures are acceptable, (3) all fonts and special characters are correct, and (4) all text and figures fit within the margin lines shown on this review document. Return to your MySPIE ToDo list and approve or disapprove this submission.

3.2 *In vitro* and *in vivo* TPL imaging with gold nanorods

Imaging modalities based on nonlinear optical effects such as TPL have some significant advantages over conventional imaging methods based on resonant light backscattering or linear fluorescence. Linear optical recordings are essentially limited to lateral imaging in the *x*-*y* plane, whereas TPL signals are also resolved along the axial direction because of their nonlinear dependence on the excitation intensity, thereby providing 3D spatial resolution. In our studies, the FWHM of the lateral and axial TPL intensity profiles from a single gold nanorod were estimated to be 0.3 and 1.0 μm, respectively.[11] Furthermore, the background fluorescence of biological tissues by multiphoton excitation is very low and permits much higher signal-to-noise ratios than conventional optical imaging, and the power densities required for TPL excitation are well below the damage threshold of biological tissue. The low background noise of TPL imaging is particularly useful for monitoring biological processes in real time. This is illustrated below by monitoring the uptake of gold nanorods by KB cells using single-particle tracking analysis,[21] and by *in vivo* imaging of gold nanorods passing through the blood vessels in a mouse earlobe.[11]

3.2.1 *In vitro* TPL imaging. We have observed that CTAB-stabilized (i.e. unfunctionalized) gold nanorods are internalized by mammalian cells within a few hours by a nonspecific uptake mechanism.[21] Nanorod uptake under these conditions is presumed to be driven by the action of CTAB on the cell membranes, rather than by endocytosis induced by serum proteins adsorbed on the nanoparticle surface.[22] Adherent KB cells (a tumor cell line derived from oral epithelium) were treated with a washed solution of nanorods in serum-free RPMI growth medium, and maintained under standard cell growth conditions prior to examination with a confocal laser scanning microscope. TPL images were obtained after a 24-h incubation period at different focal depths, confirming that the majority of the nanorods were internalized and had migrated toward the perinuclear region (see Figure 4a). A linescan of the TPL signals in Figure 4a demonstrates the high signal-to-background ratio produced by nanorods inside the KB cells (see Figure 4b).

In order to obtain additional insights into the mechanism of nanorod uptake, single-particle tracking (SPT) analysis[23] was performed to measure the trajectory and velocity of the internalized nanorods (see Figure 4c-f).[21] A nanorod positioned initially near the outer membrane exhibited bidirectional motion over a 60-s interval with overall momentum toward the nucleus, with an average velocity of 23 nm/s and a diffusion rate of 420 nm^2/s. The quadratic time-dependent term in the nanorod's mean squared displacement (MSD) is consistent with a directed motion model, and strongly suggestive of vesicular transport. We surmise that the activity of CTAB is similar to that of cationic transfection agents, which have also been shown to mediate nanoparticle uptake in mammalian cells.[24]

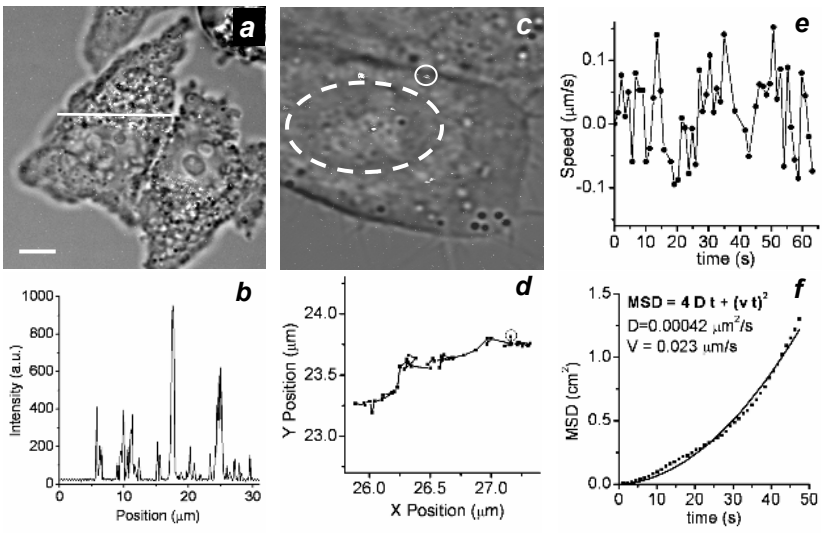

Figure 4. (a) Overlay of transmission and TPL images of CTAB-stabilized gold nanorods internalized by KB cells after a 24-h incubation (bar = 10 μm). (b) TPL intensity profile across white line in *a*. (c,d) SPT analysis and trajectory of a single nanorod (in solid circle) migrating toward the nucleus (in dashed ellipse) over a 60-s interval. (e,f) Instantaneous velocity and mean squared displacement (MSD) of nanorod signal; + and – values indicate motion toward and away from the cell nucleus, respectively. Reprinted with permission from the American Chemical Society.

SPIE USE: ____ DB Check, ____ Prod Check, Notes:

Please verify that (1) all pages are present, (2) all figures are acceptable, (3) all fonts and special characters are correct, and (4) all text and figures fit within the margin lines shown on this review document. Return to your MySPIE ToDo list and approve or disapprove this submission.

3.2.2. *In vivo* TPL imaging. Picomole quantities of CTAB-coated gold nanorods (λ_{LPR}=830 nm) were introduced into an anesthetized Balb/C mouse by tail vein injection, then detected in the vasculature several minutes later by monitoring two blood vessels in an earlobe.[11] Nanorods passing through the field of view were imaged in real time using fs-pulsed excitation centered on their longitudinal plasmon resonance (see Figure 5). The intensities of the TPL signals in single-frame images were found to be relatively uniform, indicating that most of these were produced by individual nanorods. The TPL signals were several times stronger than the autofluorescence generated by blood or the surrounding tissue, save for some isolated pockets (possibly associated with melanin in hair follicles). It is worth noting that exogenous TPL signals could no longer be detected after approximately 30 minutes, indicating that the unfunctionalized nanorods had been cleared from the bloodstream. Issues concerning rapid clearance or cell-specific targeting may be addressed by appropriate modification of the nanorod surface, as will be discussed in the next section.

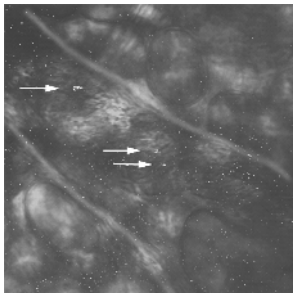

Figure 5. Still-frame TPL image of gold nanorods (indicated by white arrows) passing through a mouse ear vein, several minutes following tail vein injection (blood vessel lining enhanced for clarity). Reprinted with permission from the National Academy of Sciences.

3.3 Integrated imaging and therapy with functionalized gold nanorods

The nanorods' capacity to serve as TPL-based imaging agents is complemented by their efficient conversion of NIR optical energy into thermal energy, suggesting applications in image-guided photothermolysis. A recent study measured rapid increases in temperature upon irradiating nanorods at plasmon resonance using 20 mW at the sample, with $\Delta T = 26$ °C after 5 min for an aqueous dispersion and $\Delta T > 75$ °C after just 1 min for nanorods embedded in media of low thermal conductivity such as polyurethane.[25] The possibility of coupling TPL imaging with photothermal therapy is attractive as a noninvasive alternative to surgery: generation of hyperthermia in diseased tissues can compromise the cells' resistance to chemotherapy or radiation, or result in necrosis at higher temperatures.[26] Several examples of *in vitro* and *in vivo* photothermal therapy mediated by plasmon-resonant nanoparticles have been recently reported.[2,5,10,27]

3.3.1 Hyperthermic effects of gold nanorods. The photothermal effects of gold nanorods internalized by KB cells was demonstrated by switching the Ti:sapphire laser from fs-pulsed to continuous-wave (cw) mode, then irradiating select cells for 30 s under scanning conditions at incident laser powers ranging from 7.5−60 mW at the sample (see Figure 6).[14] These cells suffered extensive membrane blebbing at incident powers as low as 15 mW, corresponding to an approximate laser fluence of 30 J/cm^2. The cells were also positively stained by ethidium bromide, a dye used as an indicator of membrane permeability and loss of cell viability. As a control, untreated KB cells were irradiated for 30 seconds at 60 mW, with no visible evidence of hyperthermic injury.

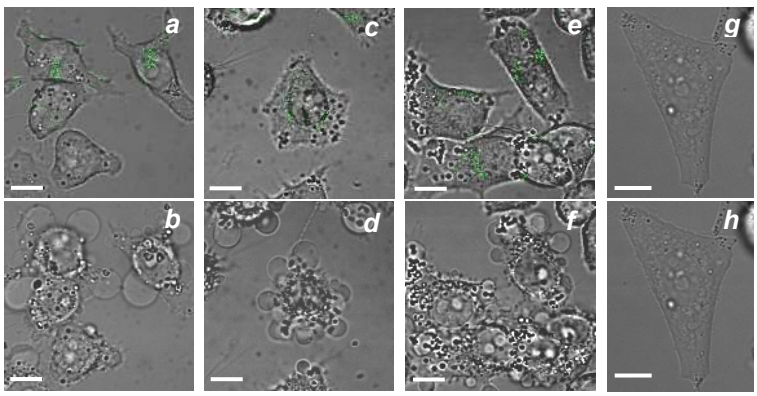

Figure 6. Nanorod-mediated hyperthermia of KB cells using cw-NIR irradiation (λ_{inc}= 795 nm, 30 s exposure) at various incident powers. KB cells with internalized nanorods before and after irradiation at 60 mW (*a*, *b*), 30 mW (*c*, *d*), and 15 mW (*e*, *f*). Severe blebbing of the cell membranes and loss of nanorod TPL signals was observed in all three cases. No changes were observed for KB cells without nanorods, before or after 60 mW irradiation (*g*, *h*). Bar = 10 μm. Reprinted with permission from Future Medicine, Ltd.

SPIE USE: ____ DB Check, ____ Prod Check, Notes:

Please verify that (1) all pages are present, (2) all figures are acceptable, (3) all fonts and special characters are correct, and (4) all text and figures fit within the margin lines shown on this review document. Return to your MySPIE ToDo list and approve or disapprove this submission.

The photothermal effects of plasmon-resonant nanorods on cells have both positive and negative consequences for clinical imaging applications. Although the nanorods have obvious potential as multimodal imaging and therapeutic agents, their preclinical evaluation is necessary to determine if their adsorption, distribution, metabolism, excretion, and toxicity (ADME/T) profiles fall within an acceptable range. In particular, the nonspecific cell uptake of CTAB-coated nanorods raises concerns over their clinical use, as it may interfere with site-specific imaging or inflict collateral injury on healthy cells if applied as photothermal agents. Therefore, *in vivo* biomedical applications involving nanorods will likely require the complete removal of CTAB to safeguard against nonspecific uptake and accumulation, and surface bioconjugation to mediate dispersion stability, extended circulation lifetimes, and targeted delivery toward diseased cells and tissues.

3.3.2 Functionalized gold nanorods via *in situ* DTC formation. Surface functionalization is a critical issue in the development of gold nanorods and other nanoparticles for applications in site-directed targeted imaging or therapy. Some of the more widely used methods for nanoparticle functionalization include the electrostatic physisorption of proteins and other biomolecules[28] and the chemisorption of thiolated ligands.[29] Both methods have the benefit of simplicity, but suffer from serious limitations in stability: the forces involved are typically weak and the adsorbed molecules are prone to desorption by competing polyelectrolytes. In the case of thiol adsorption, it has been shown that even well-packed monolayers of alkanethiols are not sufficiently robust to survive physiological conditions for long periods of time: the ligands can spontaneously desorb from surfaces as disulfides,[30] or be displaced by biogenic thiols such as cysteine or glutathione.[31] In fact, water-soluble thiols such as mercaptoethanol are often used to displace thiol-functionalized gold surfaces by simple ligand exchange, which goes to completion within a matter of hours.[32]

We have recently established that dithiocarbamates provide a robust alternative to thiols for surface functionalization,[15] and may provide a suitable platform for preparing functionalized metal nanoparticles with favorable ADME characteristics. DTC ligands can be prepared *in situ* by condensing CS_2 with primary or secondary amines, and have superior chemisorption to gold surfaces under physiological conditions while retaining the simplicity of self-assembly. In the case of the gold nanorods, exchanging the preexisting CTAB coating with mPEG-DTC (see Section 2.1) produced nanorod dispersions which were stable in biological media and inert to cell uptake. Using identical incubation conditions, the uptake rate of mPEG-DTC-coated nanorods by KB cells was only 6% relative to that of CTAB-coated nanorods.[13]

Folate-conjugated nanorods with OEG spacers were also prepared by *in situ* DTC formation followed by membrane dialysis for removal of residual CTAB, then evaluated for selective binding and uptake by KB cells, which are known to overexpress folate receptors.[14] We observed a drastic reduction in cell uptake: although the folate-conjugated nanorods readily accumulated on cell membranes, they were not rapidly internalized but remained at the cell surface for many hours (see Figure 7a). The targeted nature of nanorod binding has been confirmed by the observation that folate-conjugated nanorods were not internalized by NIH-3T3 cells, which lack high-affinity folate receptors.[33]

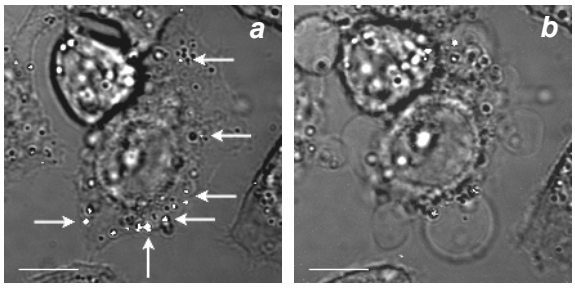

Figure 7. (*a*) Overlay of transmission and TPL images of folate-conjugated nanorods (marked with arrows) bound to KB cells after 5 h incubation; (b) KB cells after cw-NIR irradiation at 50 mW (λ_{inc}= 795 nm, 30 s exposure). Bar = 10 μm. Reprinted with permission from Future Medicine, Ltd.

KB cells incubated with folate-conjugated nanorods were also exposed to cw-NIR irradiation and evaluated for photothermal damage (see Figure 7b).[14] Again, the cells suffered extensive membrane blebbing after a 30-s exposure and could be stained by ethidium bromide, which demonstrates that the nanorods do not need to be fully internalized by cells to mediate photothermal damage. It is worth mentioning that cell photothermolysis was also accompanied by loss of TPL activity, indicating degradation of gold nanorods at high laser power. Studies are currently in progress to establish the threshold laser fluence needed to inflict nanorod-mediated cell damage, as well as the mechanistic basis of membrane blebbing; recent observations indicate that hyperthermic effects can be induced at much lower fluences when the nanorods are localized on the cell membrane, which appears to be the region most susceptible to thermal ablation.[33,34]

SPIE USE: ____ DB Check, ____ Prod Check, Notes:

Please verify that (1) all pages are present, (2) all figures are acceptable, (3) all fonts and special characters are correct, and (4) all text and figures fit within the margin lines shown on this review document. Return to your MySPIE ToDo list and approve or disapprove this submission.

4. CONCLUSIONS

Plasmon-resonant gold nanorods provide excellent contrast for TPL-based imaging and are also highly effective at transducing NIR light into heat, and are thus promising as multifunctional agents for image-guided therapies based on localized photothermolysis. Nanorods can be targeted directly to the membranes of tumor cells by removing adventitious CTAB to minimize nonspecific cell uptake, and by using *in situ* dithiocarbamate formation for the robust attachment of ligands with high affinity for overexpressed cell-surface receptors. Nanorod-mediated heating produces severe blebbing in cell membranes, and renders them permeable to chemical agents.

ACKNOWLEDGEMENTS

Acknowledgments. This work was supported by the National Institutes of Health (EB-001777), the National Science Foundation (CHE-0243496), and a grant from the Oncological Sciences Center at Purdue University. The authors thank Prof. Phil Low and Mr. Wei He for providing KB cells and collaborations involving *in vivo* imaging, and Mr. Hongtao Chen for his assistance in SPT analysis.

REFERENCES

[1] Helmchen, F., and Denk, W. (2005). Deep tissue two-photon microscopy. Nature Methods *2*, 932-40.

[2] Loo, C., Lowery, A., West, J., Halas, N., and Drezek, R. (2005). Immunotargeted nanoshells for integrated cancer imaging and therapy. Nano Lett. *5*, 709-11.

[3] Wang, Y., Xie, X., Wang, X., Ku, G., Gill, K. L., O'Neal, D. P., Stoica, G., and Wang, L. V. (2004). Photoacoustic tomography of a nanoshell contrast agent in the in vivo rat brain. Nano Lett. *4*, 1689-92.

[4] Chen, J., Saeki, F., Wiley, B. J., Cang, H., Cobb, M. J., Li, Z.-Y., Au, L., Zhang, H., Kimmey, M. B., Li, X., and Xia, Y. (2005). Gold nanocages: bioconjugation and their potential use as optical imaging contrast agents. Nano Lett. *5*, 473-77.

[5] (a) Huang, X., El-Sayed, I. H., Qian, W., and El-Sayed, M. A. (2006). Cancer cell imaging and photothermal therapy in the near-infrared region by using gold nanorods. J. Am. Chem. Soc. *128*, 2115-20. (b) Takahashi, H., Niidome, T., Nariai, A., Niidome, Y., and Yamada, S. (2006). Gold nanorod-sensitized cell death: Microscopic observation of single living cells irradiated by pulsed near-infrared laser light in the presence of gold nanorods. Chem. Lett. *35*, 500-01.

[6] Sönnichsen, C., Franzl, T., Wilk, T., von Plessen, G., Feldmann, J., Wilson, O., and Mulvaney, P. (2002). Drastic reduction of plasmon damping in gold nanorods. Phys. Rev. Lett *88*, 077402.

[7] (a) Jana, N. R., Gearheart, L., and Murphy, C. J. (2001). Seed-mediated growth approach for shape-controlled synthesis of spheroidal and rod-like gold nanoparticles using a surfactant template. Adv. Mater. *13*, 1389-93. (b) Sau, T. K., and Murphy, C. J. (2004). Seeded high yield synthesis of short Au nanorods in aqueous solution. Langmuir *20*, 6414-20.

[8] Nikoobakht, B., and El-Sayed, M. A. (2003). Preparation and growth mechanism of gold nanorods (NRs) using seed-mediated growth method. Chem. Mater. *15*, 1957-62.

[9] Zweifel, D. A., and Wei, A. (2005). Sulfide-arrested growth of gold nanorods. Chem. Mater. *17*, 4256-61.

[10] Hirsch, L. R., Stafford, R. J., Bankson, J. A., Sershen, S. R., Rivera, B., Price, R. E., Hazle, J. D., Halas, N. J., and West, J. L. (2003). Nanoshell-mediated near-infrared thermal therapy of tumors under magnetic resonance guidance. Proc. Natl. Acad. Sci. USA *100*, 13549-54.

[11] Wang, H., Huff, T. B., Zweifel, D. A., He, W., Low, P. S., Wei, A., and Cheng, J.-X. (2005). *In vitro* and *in vivo* Two-Photon Luminescence Imaging of Single Gold Nanorods. Proc. Natl. Acad. Sci. USA *102*, 15752-56.

[12] Bouhelier, A., Bachelot, R., Lerondel, G., Kostcheev, S., Royer, P., and Wiederrecht, G. P. (2005). Surface plasmon characteristics of tunable photoluminescence in single gold nanorods. Phys. Rev. Lett *95*, 267405.

[13] Huff, T. B., Hansen, M. H., Zhao, Y., Cheng, J.-X., and Wei, A. (2007). Controlling the cellular uptake of gold nanorods. Langmuir *23*, in press (la062642r).

[14] Huff, T. B., Tong, L., Zhao, Y., Hansen, M. H., Cheng, J.-X., and Wei, A. (2007). Hyperthermic Effects of Gold Nanorods on Tumor Cells. Nanomedicine *2*, in press.

[15] Zhao, Y., Pérez-Segarra, W., Shi, Q., and Wei, A. (2005). Dithiocarbamate Assembly on Gold. J. Am. Chem. Soc. *127*, 7328-29.

SPIE USE: ____ DB Check, ____ Prod Check, Notes:

Please verify that (1) all pages are present, (2) all figures are acceptable, (3) all fonts and special characters are correct, and (4) all text and figures fit within the margin lines shown on this review document. Return to your MySPIE ToDo list and approve or disapprove this submission.

[16] (a) Balasubramanian, R., Kim, B., Tripp, S. L., Wang, X., Lieberman, M., and Wei, A. (2002). Dispersion and stability studies of resorcinarene-encapsulated gold nanoparticles. Langmuir *18*, 3676-81. (b) Kim, B., Carignano, M. A., Tripp, S. L., and Wei, A. (2004). Cluster Size Analysis of Two-Dimensional Order in Colloidal Gold Nanoparticle Arrays. Langmuir *20*, 9360-65.

[17] El-Sayed, I. H., Huang, X., and El-Sayed, M. A. (2005). Surface plasmon resonance scattering and absorption of anti-EGFR antibody conjugated gold nanoparticles in cancer diagnostics: applications in oral cancer. Nano Lett. *5*, 829-34.

[18] Mooradian, A. (1969) Photoluminescence of Metals. Phys. Rev. Lett. *22*, 185-87.

[19] Boyd, G. T., Yu, Z. H., and Shen, Y. R. (1986) Photoinduced luminescence from the noble metals and its enhancement on roughened surfaces. Phys. Rev. B *33*, 7923-36.

[20] Albota, M. A., Xu, C. and Webb, W. W. (1998). Two-Photon Fluorescence Excitation Cross Sections of Biomolecular Probes from 690 to 960 nm. Appl. Opt. *37*, 7352-56.

[21] Huff, T. B., Hansen, M. H., Zhao, Y., Cheng, J.-X., and Wei, A. (2007). Controlling the cellular uptake of gold nanorods. Langmuir *23*, in press (la062642r).

[22] Chithrani, B. D., Ghazani, A. A., and Chan, W. C. W. (2006). Determining the Size and Shape Dependence of Gold Nanoparticle Uptake into Mammalian Cells. Nano Lett. *6*, 662-68.

[23] Saxton, M. J., and Jacobson, K. (1997) Single-Particle Tracking: Applications to Membrane Dynamics. Annu. Rev. Biophys. Biomol. Struct. *26*, 373-99.

[24] (a) Zhao, Y., Sadtler, B., Min, L., Hockerman, G. H., and Wei, A. (2004). Nanoprobe implantation into mammalian cells by cationic transfection. Chem. Commun., 784-85. (b) Derfus, A. M., Chan, W. C. W., and Bhatia, S. N. (2004). Intracellular Delivery of Quantum Dots for Live Cell Labeling and Organelle Tracking. Adv. Mater. *16*, 961-66.

[25] Chou, C.-H., Chen, C.-D., and Wang, C. R. C. (2005) Highly efficient, wavelength-tunable, gold nanoparticle based optothermal nanoconvertors, J. Phys. Chem. B *109*, 11135-38.

[26] Wust, P., Hildebrandt, B., Sreenivasa, G., Rau, B., Gellerman, J., Riess, H., Felix, R., and Schlag, P. M. (2002). Hyperthermia in combined treatment of cancer. The Lancet Oncology *3*, 487-97.

[27] (a) Pitsillides, C. M., Joe, E. K., Wei, X., Anderson, R. R., and Lin, C. P. (2003) Selective cell targeting with light-absorbing microparticles and nanoparticles, Biophys. J. *84*, 4023-32. (b) Zharov, V. P., Mercer, K. E., Galitovskaya, E. N., and Smeltzer, M. S. (2005) Photothermal nanotherapeutics and nanodiagnostics for selective killing of bacteria targeted with gold nanoparticles, Biophys. J. *90*, 619-27.

[28] Hayat, M. A. (1989). Colloidal Gold: Principles, Methods, and Applications. Vol 1 (San Diego, Academic Press).

[29] (a) Templeton, A. C., Wuelfing, M. P., and Murray, R. W. (2000). Monolayer protected cluster molecules. Acc. Chem. Res. *33*, 27-36. (b) Love, J. C., Estroff, L. A., Kriebel, J. K., Nuzzo, R. G., and Whitesides, G. M. (2005). Self-Assembled Monolayers of Thiolates on Metals as a Form of Nanotechnology. Chem. Rev. *105*, 1103-70.

[30] Schlenoff, J. B., Li, M., and Ly, H. (1995) Stability and Self-Exchange in Alkanethiol Monolayers. J. Am. Chem. Soc. *117*, 12528-36.

[31] Flynn, N. T., Tran, T. N., Cima, M. J., and Langer, R. (2003) Long-term stability of self-assembled monolayers in biological media. Langmuir *19*, 10909-15.

[32] (a) Demers, L. M., Mirkin, C. A., Mucic, R. C., Reynolds, R. A., III, Letsinger, R. L., Elghanian, R., and Viswanadham, G. (2000) A Fluorescence-Based Method for Determining the Surface Coverage and Hybridization Efficiency of Thiol-Capped Oligonucleotides Bound to Gold Thin Films and Nanoparticles. Anal. Chem. *72*, 5535-5541. (b) Castelino, K., Kannan, B., and Majumdar, A. (2005) Characterization of grafting density and binding efficiency of DNA and proteins on gold surfaces, Langmuir *21*, 1956-1961.

[33] Tong, L., Zhao, Y., Huff, T. B., Hansen, M. H., Wei, A., and Cheng, J.-X. (2007). Manuscript in preparation.

[34] Zharov, V. P., Galitovskaya, E. N., Johnson, C., and Kelly, T. (2005). Synergistic enhancement of selective nanothermolysis with gold nanoclusters: potential for cancer therapy. Lasers Surg. Med. *37*, 219-26.

SPIE USE: ____ DB Check, ____ Prod Check, Notes: